Heat Transfer Engineering, 33(14):1177–1187, 2012

ISSN: 0145-7632 print / 1521-0537 online
DOI: 10.1080/01457632.2012.677695

Taylor & Francis
Taylor & Francis Group

Thermal Simulation of a Pulsating Heat Pipe: Effects of Different Liquid Properties on a Simple Geometry

MAURO MAMELI,[1] MARCO MARENGO,[1] and STEFANO ZINNA[2]

[1]Department of Industrial Engineering, University of Bergamo, Dalmine (BG), Italy
[2]Uniheat S.r.l., Bagnatica (BG), Italy

The pulsating heat pipe (PHP) is essentially a two-phase heat transfer device for low heat power applications (heat sinks, electronic cooling, etc.). Although it is a simple, cheap, and flexible structure, it is ruled by very complex physics, and a robust, validated simulation tool is still missing. In the present work the basic numerical model by Holley and Faghri (2005) has been updated with the latest fluid properties database and with the latest nondimensional heat transfer correlations in order to make it suitable for different working fluids. Good agreement between numerical results and experimental data coming from a single-loop PHP operating with ethanol is shown and, using a single "tuning" parameter, that is, the liquid film thickness around a vapor slug, which needs to be further experimentally investigated, the final goal of building a design tool for the PHP construction and implementation is getting closer.

INTRODUCTION

The sintered porous wick heat pipe technology is already successfully implemented in many industrial thermal management applications [1], but since the early 1990s a new type of wickless heat pipe prototype has been introduced by Akachi and co-workers [2–4]: the pulsating heat pipe (PHP).

It usually consists of a small-diameter meandering copper tube that can be closed in a loop (CLPHP) or with closed ends (CEPHP), evacuated, and then filled with a working fluid. Due to the capillary diameter (usually between 1 and 2 mm) the fluid fills the tube with an alternation of liquid slugs and vapor bubbles. Once the device gets in contact with a heat source, evaporation occurs and the fluid starts oscillating and circulating chaotically, allowing heat to be transported to the colder zone.

Many experimental works in literature show that a PHP could manage a wide range of industrial applications with the unquestionable advantage of being cheaper and more flexible.

Table 1 shows the comparison between the PHP and the wicked heat pipes features.

Address correspondence to Professor Marco Marengo, Department of Industrial Engineering, University of Bergamo, Viale Marconi 5, 24044 Dalmine (BG), Italy. E-mail: marco.marengo@unibg.it

Yang et al. [5] showed the possibility of embedding the PHP as an integrated structure or heat spreader, in order to provide a higher overall thermal conductance to the host substrate. The influences of various operating parameters, including volumetric filling ratio of the working fluid, input heat flux, and operating orientation, on the thermo-hydrodynamic performance, were investigated and a successful operation at all orientations with respect to gravity was achieved.

Miyazaki [6] developed a series of flexible CLPHP for notebook cooling able to dissipate heat from the central processing units (CPUs) to the rear surface of the foldable display. The wing type design with 1.2-mm channel diameter and 12 turns achieved a thermal conductance of 3.5 W/K and a maximum heat transport capability of 100 W, which are reasonably thought to be of sufficient potential for such application.

Rittidech and Wannapakne [7] investigated a flat-plate solar collector in conjunction with a CEPHP operating with R134a as a working fluid, suggesting that this solution represents a reasonably efficient and cost-effective alternative to the conventional heat pipe solar collector system with the additional advantages of corrosion-free operation and absence of icing problems during winter.

Khandekar [8] analyzed two kinds of PHP-based heat exchangers: a temperature-controlled liquid–liquid module suitable for process waste heat recovery, and a heat flux-controlled

Table 1 Comparison between wicked heat pipe and the PHP outstanding features

	Wicked HP	Pulsating HP
Temperature range	Wide, water: 30–230°C	Medium, water: 50–160°C
Radial heat flux	Very high, up to 250 W/cm^2	Medium, up to 30 W/cm^2
Axial heat flux	High, up to 600 W/cm^2	High, up to 1200 W/cm^2
Total power (strong dependence from geometry)	Medium, up to 200 W per unit	High, up to 3000 W
Thermal resistance	Very low, down to 0.01°C/W	Low, down to 0.1°C/W
Startup time	Fast, in the order of seconds	Medium, a few minutes

air-cooled module that can handle high-power electronics applications. Both the devices could reach a maximum heat throughput of 800 W, and overall thermal resistances have been found to be of the order of 0.2°C/W or lower.

In spite of its simple structure, the PHP working principles are very complex and a complete and validated design tool has not been developed yet. Looking at the present research literature, many attempts of theoretical modeling have been carried out in the last two decades but only a few ones seem to be suitable to a correct estimation of different PHPs. For instance, recently Zuo et al. [9] proposed their last version of one dimensional model for the thermal hydraulic simulation of a pulsating heat pipe. Experimental validation is shown only for the thermal performance over filling ratio, and it is not clear how a smooth tube PHP model was validated since experimental data are for a flat-plate PHP with embedded porous wick. Shafii et al. [10] presented a similar Lagrangian multiplug model with heat transfer both for the CEPHP and for the CLPHP. Although the authors consider many characteristic parameters, results show that gravity has no significant effect on the performance of CEPHP in top heat mode (i.e., with the heater in the upper part of the PHP) and that the total number of vapor plugs always reduced to the total number of heating sections, which is in contrast with experimental evidence. Zhang and Faghri [11] proposed a multiplug model of CEPHP and investigated the effect of the number of turns on the fluid oscillation frequency. Recently Sakulchangsatjatai et al. [12] considered one reviewed CEPHP model embedding the worthy results by Shafii et al. [10] and by Zhang and Faghri [11]. Furthermore, they added empirical assumptions on nucleate boiling frequency, bubble length, and film thickness coming from an experimental visualization. Qualitative and quantitative validation was given for evaporator temperatures, inclination angles, and input heat fluxes; Khandekar and Groll [13] suggested a lumped parameters model for the CLPHP (single loop), but the assumption of homogeneous fog flow seems more suitable for thermosyphons than for the PHP. The numerical code by Holley and Faghri [14] represents a good starting point for the creation of a most comprehensive tool, even if it has been tested only for water as working fluid and a only a qualitative validation is provided.

In the work here the model just described has been deeply modified both in the input parameters (geometry, boundary conditions etc.) and in the heat transfer subroutines, to achieve two main targets:

1. Let the model work with different fluids.
2. Simulate Khandekar and Groll [15] experiments and attempt a quantitative validation.

The main objection moved to Holley and Faghri [14] is the assumption of a porous wick deposited on the inner tube wall. The PHP prototype developed by Zuo et al. [9] is one of the few PHPs that combines the capillary effect of sintered metal powder wicks with the thermally induced pulsating motion of the working fluid and shows a maximum heat flux capability of 220 W/cm^2, but the very great majority of the pulsating heat pipe prototypes and experimental apparatus are built with smooth tubes.

The internal two-phase phenomena, such as the flow boiling onset, slug and plugs formation, and the flow patterns at various heat inputs, are different if the wick structure is absent and the maximum heat flux capability of the evaporator surface is always less than 30 W/cm^2.

Elimination of the wick assumption in reference [14] and the implementation of different working fluids led to a complete reconsideration of the heat transfer modeling strategy.

NUMERICAL MODEL

The present work adopts the Holley and Faghri [14] one-dimensional separated flow model as a starting scheme: The tube wall control volumes are treated with an Eulerian approach, while the fluid control volumes follow the liquid slugs and vapor plugs, which are moving with respect to the wall and are always traceable during the simulations.

The main assumptions are:

a. Spatial and time derivatives of density and viscosity are assumed negligible. However, all the fluid thermophysical properties are evaluated as functions of temperature in saturated conditions.
b. The advection term is neglected in the momentum equation for the liquid slug.
c. The model is one-dimensional (1-D) and only the axial flow path direction is considered for momentum and heat transfer, while heat transfer occurs in both the axial and radial direction.

d. The forward and backward menisci of the liquid slugs are assumed to maintain a spherical meniscus shape with zero contact angles at the wall.
e. Surface tension is evaluated at the vapor plugs temperature.
f. The pressure within each vapor plug is assumed uniform.
g. Vapor exists at saturated conditions; each vapor plug (VP) is treated as an ideal gas and has negligible flow friction.
h. The liquid film that surrounds each VP is only considered for thermodynamic purposes but does not play any role in the hydrodynamics behavior.

The governing equations are listed next.

Momentum Equation for the i-th Liquid Slug

The momentum equation for incompressible flow in a circular pipe is:

$$\rho \frac{Du_l}{Dt} = \rho g \cos\theta - \frac{dP}{dz} + \frac{\tau}{d} \tag{1}$$

where $\frac{Du_l}{Dt} = \frac{\partial u_l}{\partial t} + u_l \frac{\partial u_l}{\partial z}$ is the total derivative. By means of assumptions (a) and (b), writing the slug velocity as

$$u_l = \dot{m}_l / \rho A_{cr} \tag{2}$$

and integrating along the liquid slug length, the momentum equation turns into the following ordinary differential equation, which is applied to each i-th liquid slug:

$$\left[\frac{d\dot{m}_l}{dt} = A_{cr}(\Delta P_g - \Delta P_v + \Delta P_\tau) \right]_i \tag{3}$$

Note that the liquid slug is treated with a lumped parameter approach. The liquid slug will be subdivided into a number n_s of smaller control volume only for solving the energy equation (see energy equation for the liquid slug).

The different pressure terms on the right-hand side are respectively due to:

Gravity force:

$$\Delta P_g = \rho_l g \cos\theta \tag{4}$$

where theta is the angle between the gravity vector and the flow direction.

Adjacent vapor plugs expansion/compression:

$$\Delta P_v = ([P_{sat}(T_v)]_{j+1} - [P_{sat}(T_v)]_j)/L_l \tag{5}$$

Viscous shear:

$$\Delta P_\tau = \frac{f}{2d} \rho_l u_l^2 \tag{6}$$

where the friction coefficient is evaluated for the laminar and turbulent regimes as follows:

$$f = 64/\mathrm{Re}_l \quad \text{when} \quad \mathrm{Re}_l < 2000$$
$$\frac{1}{\sqrt{f}} = 1.74 - 2\log_{10}\left(\frac{2\varepsilon}{d} + \frac{18.6}{\mathrm{Re}_l\sqrt{f}}\right) \quad \text{when} \quad \mathrm{Re}_l \geq 2000 \tag{7}$$

where $\mathrm{Re}_l = \frac{\rho_l u_l d}{\mu_l}$ is the Reynolds number related to each liquid slug.

Liquid Slug Merge

The merging of liquid slugs is accounted for. If the spacing between any two adjacent menisci is zero, the two liquid slugs are combined in volume and the number of liquid slugs is reduced by one. The mass flow rate for the combined slug is determined by summing the momenta.

Vapor Plug Formation

Finally, the formation of new vapor plugs has been taken into account only in terms of pure nucleation inside the liquid phase. There are two possible criteria to generate new vapor plugs: (1) a temperature criterion and (2) a pressure criterion.

In the first case the following procedure is implemented:

- The temperature of each liquid subvolume is compared to the temperatures of the vapor plugs adjacent to the liquid slug.
- If that temperature exceeds one or the other adjacent plug temperatures, the corresponding grid is chosen as the location where a new vapor plug is formed. The two newborn slugs have the same mass flow rate.
- The temperature of the new vapor plug is set to the fluid temperature at that location.

The other criterion for locating new vapor plugs is to compare the saturation pressure associated with the liquid slug grid boundary temperature to the pressure of the adjacent vapor bubble boundary:

$$[P_{sat}(T_l)]_{n_s} > \max\left[\left(P_{sat}(T_v) + \frac{2\sigma}{r_c}\right)_j ; \left(P_{sat}(T_v) + \frac{2\sigma}{r_c}\right)_{j+1}\right] \tag{8}$$

If this condition occurs, a new vapor plug will be created, and if there is sufficient vapor pressure in the plug, the plug will grow; otherwise, it will collapse and the two adjacent liquid slugs will merge again.

The Displacements of the Back Menisci Positions

The new position of each liquid slug is calculated through the mass flow rate requiring the convergence of the following equation with a suitable time step Dt:

$$\Delta z_i = \frac{\Delta t}{2A_{cr}} \left(\frac{\dot{m} + \Delta\dot{m}}{\rho_l \left[T_l\left(z_{b,i} + \Delta z_i\right)\right]} + \frac{\dot{m}}{\rho_l \left[T_l\left(z_{b,i}\right)\right]} \right) \tag{9}$$

The initial estimate is:

$$\Delta z_i = \frac{\Delta t}{2A_{cr}} \left(\frac{\dot{m} + \Delta \dot{m}}{\rho_l [T_l(z_{b,i})]} \right) \tag{10}$$

The back meniscus position is updated:

$$z_{b,i} = z_{b,i} + \Delta z_i \tag{11}$$

The forward meniscus is calculated by mean of the conservation of mass at each time step.

Energy Equation for the i-th Liquid Slug

The following partial differential equation accounts for heat storage and axial conduction within the fluid:

$$\left[c_{p,l} \rho_l A_{cr} \frac{\partial T_l}{\partial t} = q_{w-f} p + k_l A_{cr} \frac{\partial^2 T_l}{\partial z^2} \right]_i \tag{12}$$

Each liquid slug is divided into n_s grids and the temperature for each grid is evaluated by integrating Eq. (12). The remaining spatial derivative is determined using a first-order central difference. Values of heat transfer between the wall and fluid are interpolated based on the representative values of adjacent grids.

Energy Equation for the Wall

Holley and Faghri [14] assumed that the internal tube surface is covered by a thin wick and that the liquid film surrounding each vapor bubble always filled the porous structure. Since most of the prototypes and the experimental apparatus are built with smooth tubes without any wick (this is also the most attractive feature of the CLPHP with respect to the standard heat pipe), the wick is not considered in the present work and the energy equation for the wall is:

$$c_{p,w} \rho_w A_w \frac{\partial T_w}{\partial t} = q_{ex} p_{ex} - q_{w-f} p + k_w A_w \frac{\partial^2 T_w}{\partial z^2} \tag{13}$$

where

$$q_{ex} = \begin{cases} q_{ev} & \text{evaporator zone} \\ 0 & \text{adiabatic zone} \\ h_\infty (T_\infty - T_w) & \text{condenser zone} \end{cases} \tag{14}$$

The entire wall tube is divided into n_w grids and the temperature for each wall grid is evaluated by integrating Eq. (13). The remaining spatial derivative is determined using a first-order central difference. Values of heat transfer between the wall and fluid are interpolated based on the representative values of adjacent grids.

Energy Equation for the j-th Vapor Plug

The following partial differential equation accounts for the heat storage within the entire vapor plug, for the heat transferred between vapor and the tube wall $q_{w\text{-}f}$, and for axial conduction with the neighbouring liquid slugs:

$$\left[(z_{f,j} - z_{b,j}) A_{cr} \frac{\partial}{\partial t} \left(H_g \frac{P_{sat}(T_v)}{R_v T_v} \right) = q_{w-f} p (z_{f,j} - z_{b,j}) + k_l A_{cr} \left. \frac{\partial T_l}{\partial z} \right|_{Z_{f,i-1}} - k_l A_{cr} \left. \frac{\partial T_l}{\partial z} \right|_{Z_{b,i}} \right]_j \tag{15}$$

Forward and backward first-order differences are used for conduction at the menisci.

Heat Transfer Between the Tube Wall and the Working Fluid

When the local Reynolds number related to the i-th liquid slug is $\mathrm{Re} < 2000$ and the liquid slug is heated or cooled by means of sensible heat, the local Nusselt number is far from being constant, and thus the thermally developing laminar flow correlation by Shah [16] has been implemented:

$$h_l = \begin{cases} \left(\frac{k_l}{d} \right) \cdot 1.953 \cdot \left(\mathrm{Re}_l \mathrm{Pr}_l \frac{d}{L_x} \right)^{1/3} & \text{when } \left(\mathrm{Re}_l \mathrm{Pr}_l \frac{d}{L_x} \right) \geq 33.3 \\ \left(\frac{k_l}{d} \right) \left(4.364 + 0.0722 \mathrm{Re}_l \mathrm{Pr}_l \frac{d}{L_x} \right) & \text{when } \left(\mathrm{Re}_l \mathrm{Pr}_l \frac{d}{L_x} \right) \leq 33.3 \end{cases} \tag{16}$$

where L_x is the thermal entry length and it is set equal to the evaporator/condenser length.

For the transient/turbulent flow ($2000 \leq \mathrm{Re}_l \leq 10{,}000$) the Gnielinski correlation [17] has been implemented:

$$h_l = \left(\frac{k_l}{d} \right) \left[\frac{(f/8)\left(\mathrm{Re}_l - 10^3\right) \mathrm{Pr}_l}{1 + 12.7 (f/8)^{1/2} \left(\mathrm{Pr}_l^{2/3} - 1 \right)} \right] \tag{17}$$

For the fully turbolent flow ($\mathrm{Re}_l \geq 10{,}000$) the Dittus–Boelter correlation [17] has been used:

$$h_l = \left(\frac{k_l}{d} \right) 0.023 \mathrm{Re}_l^{0.8} \mathrm{Pr}_l^n \tag{18}$$

where $n = 0.4$ if $T_{wall} > T_{fluid}$ and $n = 0.3$ if $T_{wall} < T_{fluid}$.

From the fluid mechanical point of view, the vapor plugs are made of vapor only, while from the heat transfer point of view, a thin liquid film is supposed to wet the inner tube surface sourrounding the vapor plugs and no slip exists between the phases (assumption h). Due to these hypothesis each vapor plug is hence treated as a two-phase system in equilibrium where the local vapor mass quality x_{VP} is not calculated as the ratio of mass fluxes but simply as the ratio of masses; x_{VP} is then only a function of the liquid film thickness δ_{film} and the fluid density, which depends on the fluid temperature. If δ_{film} is assumed

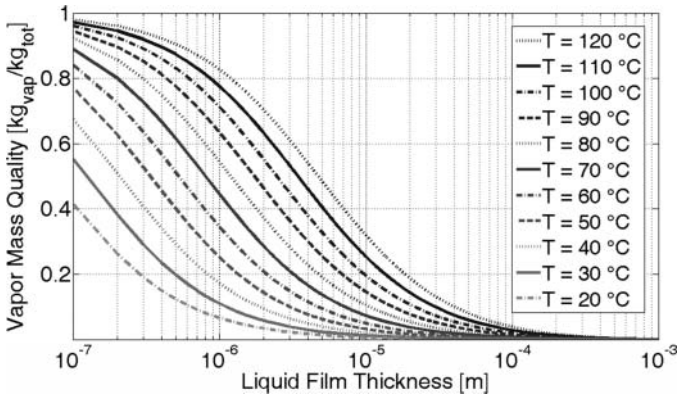

Figure 1 Vapor mass quality over liquid film thickness for different fluid temperatures (ethanol).

constant along the vapor slug, then the local vapor mass quality can be calculated as follows:

$$x_{VP} = \frac{m_v}{m_t} = \frac{V_v \rho_v (T_{sat})}{V_v \rho_v (T_{sat}) + V_l \rho_l (T_{sat})}$$

$$= \frac{\left(\frac{d}{2} - \delta_{film}\right)^2 \rho_v (T_{sat})}{\left[\left(\frac{d}{2} - \delta_{film}\right)^2 \rho_v (T_{sat})\right] + \left\{\left(\frac{d}{2}\right)^2 - \left[\left(\frac{d}{2} - \delta_{film}\right)^2\right] \rho_l (T_{sat})\right\}} \quad (19)$$

In Figure 1 the vapor mass quality has been plotted as a function of the liquid film thickness for different fluid temperatures.

If the liquid film thickness is defined, then the local vapor mass quality can be also calculated by mean of Eq. (19) and feed into the semiempirical correlations for the two phase heat transfer (Eqs. (20) and (21)). Even if δ_{film} is a crucial parameter and should not be a direct input for the code, it is also very difficult to obtain experimental data. The last available measurements by Han and Shikazono [18] for a 1.305-mm internal diameter tube working with air and ethanol in adiabatic conditions show that the valid range for δ_{film} is between 1 and 100 μm. This range has been taken as reference. In the present model the vapor mass quality (i.e., the liquid film thickness) of each vapor plug is assumed a priori on the basis of the following argument: If a vapor bubble is passing through the evaporator zone then the liquid film is subjected to relatively high temperatures and undergoes evaporation. Under these conditions (high temperature and thin liquid film due to the evaporation process), a high vapor mass quality x_{ev} can be chosen for the vapor plugs that are passing through the evaporator section. The opposite applies in the condenser zone, so the lower average fluid temperature and the thicker liquid films lead to a very low vapor mass quality x_{co}.

For the time being the liquid film thickness must be treated as a tuning parameter, which is chosen within a reasonable range extrapolated from experimental data (Table 2): once the average ranges of fluid temperature for each input heat flux $\left[T_{vp,\min} : T_{vp,\max}\right]$; are determined, the vapor mass quality ranges $\left[x_{vp,\min} : x_{vp,\max}\right]$ are calculated with respect to these temperatures using $\delta_{film,\min} = 1\mu m$ and $\delta_{film,\max} = 100\,\mu m$. The final vapor mass quality for the evaporating $x_{vp,ev}$ and condensing $x_{vp,co}$ vapor plugs have been chosen in between these ranges, as shown in Table 2.

Regarding the boiling/evaporation heat transfer, the Gungor and Winterton [19] general correlation is used:

$$h_b = h_l \left\{1 + 3000 Bo^{0.86} + \left[\frac{x_{ev}}{1 - x_{ev}}\right]^{0.75} \left(\frac{\rho_l}{\rho_v}\right)^{0.41}\right\} \quad (20)$$

where $Bo = \frac{q A_{cr}}{|\dot{m}| H_{lv}}$ is the boiling number, $x_{ev} = x_{vp,ev}$ is the vapor mass quality of the heated vapor plugs and h_l is the single-phase (liquid) convection coefficient evaluated for the different flow regimes (Eqs. (16)–(18)).

With regard to the condenser zone the standard correlation for convective condensation by Shah [20] has been implemented:

$$h_{co} = h_l \left[(1 - x_{co})^{0.8} + \frac{3.8 x_{co}^{0.76} (1 - x_{co})^{0.04}}{(P/P_{crit})}\right] \quad (21)$$

where $x_{co} = x_{vp,co}$ is the vapor mass quality of the cooled vapor plugs.

In light of the hypothesis described already, the heat transfer subroutine is set as follows.

For the liquid slugs:

- If $T_{wall} < T_{fluid}$ set boiling heat transfer correlation (HTC) (Eq. 20) with $x_{ev} = 0$. This is a limit condition where the liquid slug is assumend under incipient boilig so it is still completely liquid but heat input rate plays an important role.
- If $T_{wall} < T_{fluid}$ set single-phase liquid HTC (Eqs. (16)–(18)).

For the vapor plugs:

- If $T_{wall} < T_{fluid}$ set boiling HTC (Eq. (20)) with x_{ev} chosen with the help of Eq. (19).
- If $T_{wall} < T_{fluid}$ set condensation HTC (Eq. (21)) with x_{co} chosen with the help of Eq. (19).

Fluid Properties, Input Parameters

Dedicated subroutines for the fluid properties of interest in saturated condition $c_{p,l}(T_{sat})$; $c_{p,v}(T_{sat})$; $H_l(T_{sat})$; $H_v(T_{sat})$; $k_l(T_{sat})$; $k_v(T_{sat})$; $\mu_l(T_{sat})$; $\mu_v(T_{sat})$; $P_{sat}(T_{sat})$; P_{cr}; $\rho_l(T_{sat})$; $\rho_v(T_{sat})$; $\sigma_l(T_{sat})$; $T_{sat}(P_{sat})$ have been implemented for five different working fluids with the NIST REFPROP 8.0 [21] within the temperature ranges listed in Table 3. The input parameters (geometry, initial conditions, boundary conditions and computational parameters) have been set in order to simulate the single closed loop PHP shown in Figure 2 and they are listed in Table 4.

Table 2 Choice of the vapor mass quality for evaporating and condensing vapor plugs

$q''[W/cm^2]$																
4				8				12				16				
$T_{vp,\min}[^\circ C]$ 23		$T_{vp,\max}[^\circ C]$ 55		$T_{vp,\min}[^\circ C]$ 34		$T_{vp,\max}[^\circ C]$ 70		$T_{vp,\min}[^\circ C]$ 54		$T_{vp,\max}[^\circ C]$ 87		$T_{vp,\min}[^\circ C]$ 76		$T_{vp,\max}[^\circ C]$ 117	
$x_{vp,\min}$	$x_{vp,\max}$	$x_{vp,\min}$	$x_{vp,\max}$	$x_{vp,\min}$	$x_{vp,\max}$	$x_{vp,\min}$	$x_{vp,\max}$	$x_{vp,\min}$	$x_{vp,\max}$	$x_{vp,\min}$	$x_{vp,\max}$	$x_{vp,\min}$	$x_{vp,\max}$	$x_{vp,\min}$	$x_{vp,\max}$
0.0007	0.0772	0.0036	0.2960	0.0013	0.1320	0.0065	0.4343	0.0034	0.2867	0.0130	0.6074	0.0083	0.4944	0.0355	0.8116
$x_{vp,co}$ 0.001		$x_{vp,ev}$ 0.01		$x_{vp,co}$ 0.01		$x_{vp,ev}$ 0.1		$x_{vp,co}$ 0.1		$x_{vp,ev}$ 0.5		$x_{vp,co}$ 0.4		$x_{vp,ev}$ 0.8	

Table 3 List of the working fluids temperature ranges implemented in the numerical code

Fluid	T min (°C)	T max (°C)
Ethanol	−18	202
FC-72	2	152
Methanol	−53	197
R123	−73	167

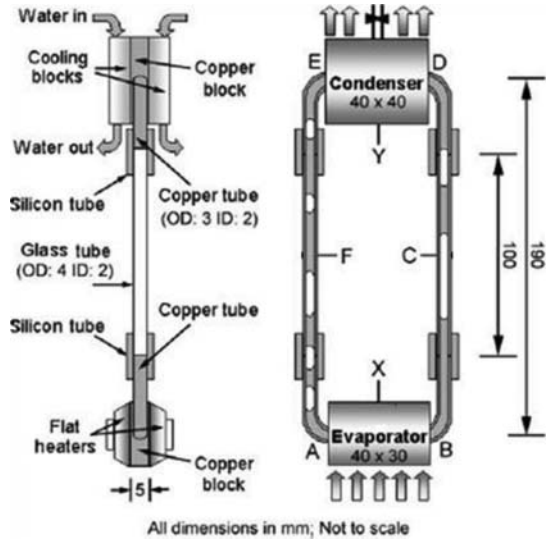

Figure 2 Scheme of single closed loop PHP built by Khandekar and Groll [15].

Table 4 Code input parameters that are constant for every simulation

Input parameter	Value
Tube thermal conductivity	400 (W/mK]
Tube specific heat capacity	389 (J/kgK)
Tube density	8960 (kg/m^3)
Internal tube diameter	2 (mm)
External tube diameter	3 (mm)
Inner surface roughness	5 μm
Evaporator section length	40 (mm)
Condenser section length	40 (mm)
Adiabatic section length	190 (mm)
Filling ratio	0.6 (—)
External cooling temperature	20 (°C)
Initial temperature (fluid and tube)	30 (°C)
Initial number of Liquid Slugs and Vapor Plugs	6 (—)
Heat inputs	14.8, 32.1, 44.2 (W)
Computational time step	0.0001 (s)
Number of grids for the wall domain	460 (—)
Number of grids for the liquid domain	225 (—)
Convergence criterion	0.001 (—)

NUMERICAL MODEL VALIDATION

Khandekar and Groll [15] built the single closed loop PHP experimental test rig shown in Figure 2 in order to investigate

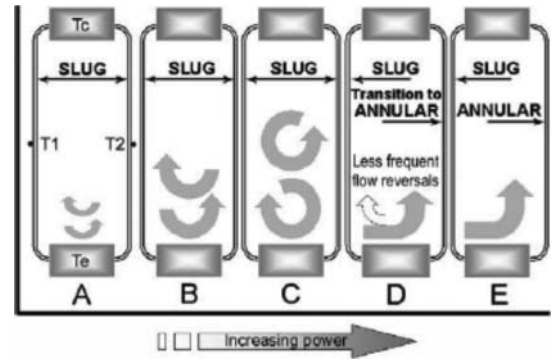

Figure 3 Single closed loop PHP thermal-hydraulic investigation by Khandekar and Groll [15].

the effect of the heat input rate on the PHP hydrodynamics and performance (Figure 3). In particular, they observed the fluid motion and flow pattern through the transparent CLPHP zone and measured the temperature trends in the evaporator and adiabatic sections. As the heat rate input is increased the flow oscillation is more active (cases A and B); then a net circulation of the fluid is more evident as well as flow reversals (case C). A further increase in the heat rate input leads to a transition of the flow pattern from complete slug flow to annular flow (cases D and E). In such final condition, liquid and vapor are separated and the device operates more likely as a thermosyphon than as a PHP.

Cases A, B, and C were simulated with the numerical code, while cases D and E were not simulated because the system does not behave anymore like a PHP: The slug flow regime is no longer present and all the liquid phase resides in one of the vertical branch while the vapor phase resides in the other. For each case the maximum tube wall temperature (Figures 4–6) and the total liquid momentum (Figures 7–9) are plotted. The end time is set to 200 s for every simulation, since for all the simulation cases the transient conditions have a shorter duration. The numerical results obtained with ethanol compares well with the PHP thermal-hydraulic behavior: Table 5 shows the mean maximum tube temperature percentage difference between measurements by Khandekar and Groll [15] and the simulations output

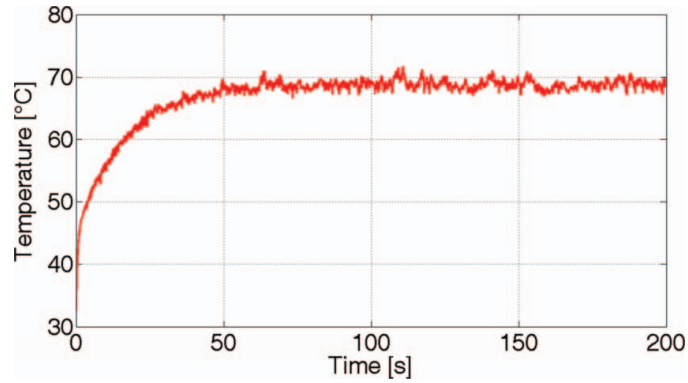

Figure 4 Numerical results: maximum tube temperature (case A, ethanol). (Color figure available online.)

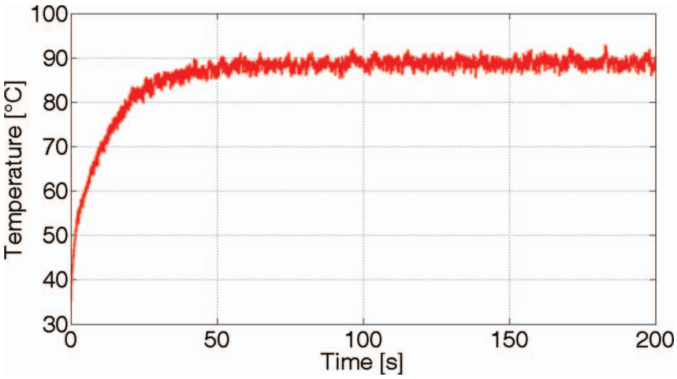

Figure 5 Numerical results: maximum tube temperature (case B, ethanol). (Color figure available online.)

values. Case D represents the transient situation between slug and annular flow regimes and it is also the limit case for the presented numerical model where the slug flow regime is assumed a priori. This fact also explains the higher error percentage between experimental data and numerical results for case C.

In one of his most recent works on the single closed loop PHP, Khandekar et al. [22] analyzed the spectral content of each quasi-steady-state pressure signal. He concluded that the dominant frequencies of flow oscillations are in the range of 0.1 to 3.0 Hz. For this reason the fast Fourier transform (FFT) analysis with a sample frequency of 20 Hz has been performed on the total liquid momentum (Figures 7–9), which is directly connected with the fluid pressure variation in time. Table 6 shows that the dominant frequencies for the three simulated cases with ethanol are within the experimental range.

Finally, in their experimental work, Yang et al. [23] demonstrated that as soon as the slug flow regime is maintained, the internal thermofluidics observed in a two-phase loop is also observed in a multiturn CLPHP. Furthermore, they also showed that the multiturn CLPHP thermal resistance can go down to 0.1 K/W, which is a very attractive value for engineering solutions. For this reason the present numerical model, which is able to simulate the thermofluid characteristics single loop closed PHP, may be the first validated step for the creation of a multiturn CLPHP design tool.

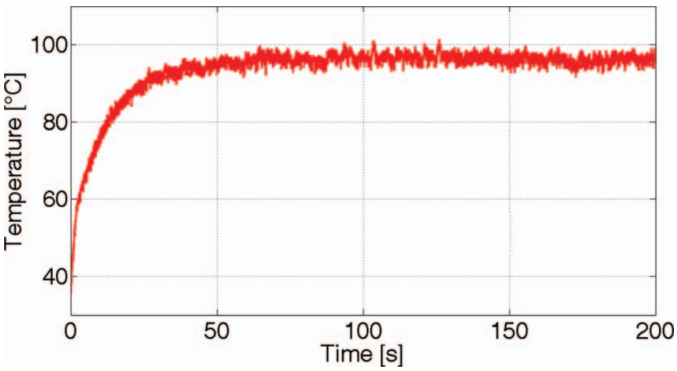

Figure 6 Numerical results: maximum tube temperature (case C, ethanol). (Color figure available online.)

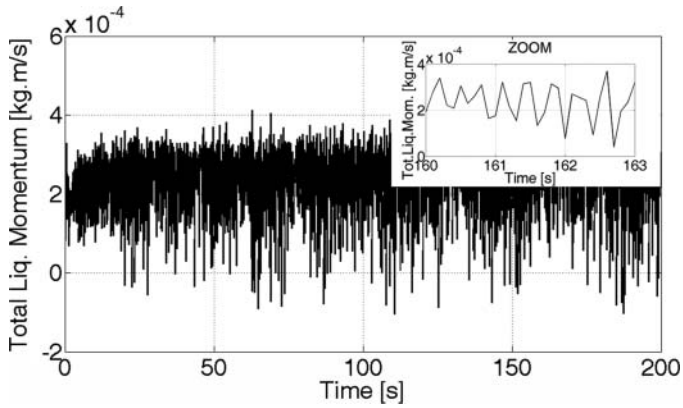

Figure 7 Numerical results: total liquid momentum (case A, ethanol).

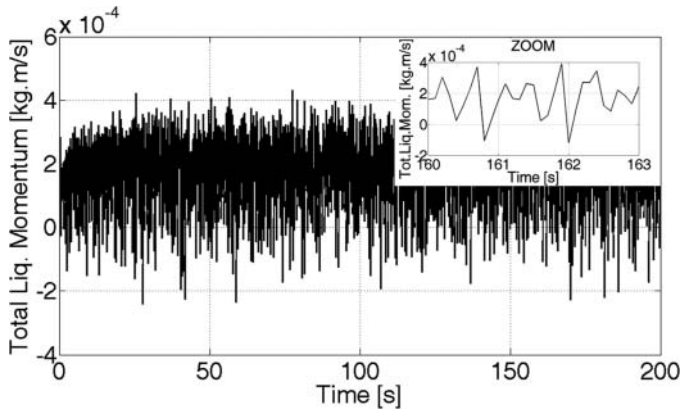

Figure 8 Numerical results: total liquid momentum (case B, ethanol).

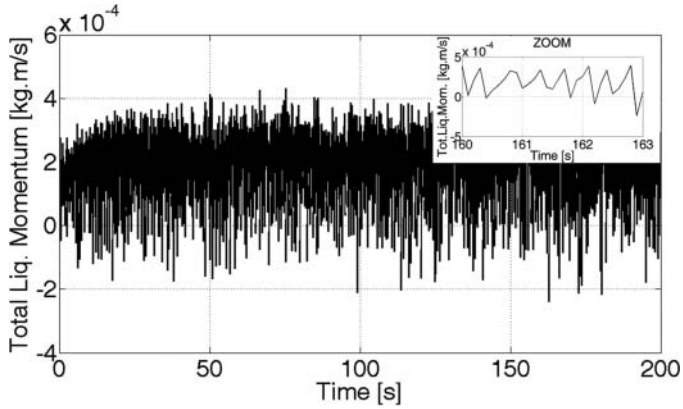

Figure 9 Numerical results: total liquid momentum (case C, ethanol).

Table 5 Mean maximum tube temperature percentage difference between the experimental data by Khandekar and Groll [15] and the simulations output values

	$\bar{T}_{w,\max}$ (exp.)	$\bar{T}_{w,\max}$(num.)	Error
Case A (14.8 W)	74.8°C	68.9°C	−7.8%
Case B (32.1 W)	83.8°C	88.9°C	6.2%
Case A (44.2 W)	84.2°C	96.5°C	14.7%

Table 6 Mass flow rate dominant frequencies for the three simulated cases with ethanol

	Dominant frequencies (Hz)
Case A (14.8 W)	2.54
Case B (32.1 W)	2.30
Case A (44.2 W)	2.24

The model input parameters were then set on the basis of the good results obtained with ethanol and the same simulations were carried forward with the fluids listed in Table 3.

Numerical results are resumed in only two plots: Figure 10 shows the mean maximum tube temperature in quasi-steady-state conditions and Figure 11 shows the PHP equivalent thermal resistance obtained with the following equation:

$$R_{eq} = \left(\bar{T}_{w,\max} - \bar{T}_{w,\min}\right)/\dot{Q} \tag{22}$$

In general the equivalent thermal resistance is in inverse proportion to the heat input level, even if it is evident from that the thermal performance is reaching an asymptotic threshold (Figure 11). From this point on, the PHP begins to work more likely as a thermosyphon and its performance is no longer enhanced by the heat input increase.

In most practical applications the evaporator temperature should be maintained under a certain threshold, and from this point of view it seems that the refrigerants fluids (FC-72 and R123) are working worse than alcohols (Figure 10). Actually the reason for such behavior is to be found in the actual temperature working range (i.e., cooling medium temperature). In this condition, the performance of the PHPs operating with refrigerants is of course lower if compared to ethanol and methanol, which are also favoued by their lower density, higher thermal conductivity, specific heat, and surface tension (Table 7). It is very likely that for applications at lower temperatures FC-72 and R123 may become more suitable and have higher performances.

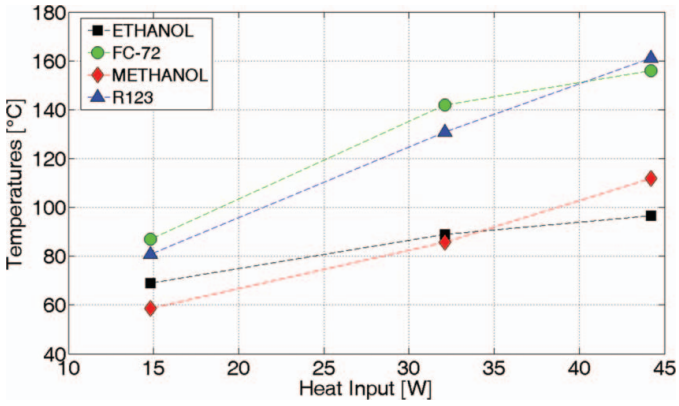

Figure 10 Numerical results: mean maximum tube temperatures in pseudo-steady state conditions. (Color figure available online.)

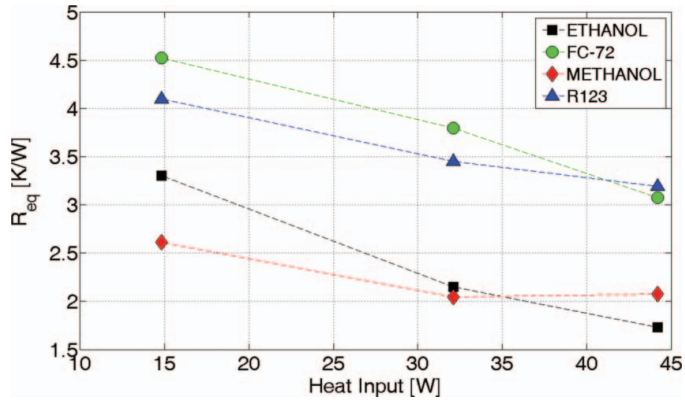

Figure 11 Numerical results: mean equivalent thermal resistances in pseudo-steady state conditions. (Color figure available online.)

Table 7 Saturated liquid properties evaluated at T = 27°C

Fluid	ρ_l	$c_{p,l}$	h_{lv}	k_l	μ_l	σ_l
Ethanol	783.82	2596.7	919, 700	0.16469	0.00104	0.02154
Methanol	784.51	2546.1	1, 166, 200	0.20018	0.00052	0.02210
FC-72	1687.6	1049.7	92, 096	0.057737	0.00064	0.01091
R123	1459.1	1021.9	170, 600	0.075902	0.00040	0.01495

CONCLUSIONS

A numerical model of a pulsating heat pipe has been implemented with different working fluids properties and a novel non-homogeneous thermodynamic approach has been developed. The basic constitutive element of a PHP (i.e., the single loop built by Khandekar and Groll [15]) has been simulated and the following conclusions can be drawn:

- The error percentage on the mean evaporator maximum temperature between numerical results and the experimental data is within the 15% despite the lack of information about the liquid film thickness that surrounds the vapor plugs in the different zones of the PHP.
- The FFT analysis that has been performed on the numerical results related to total liquid momentum, which is directly connected with the fluid pressure variation in time, confirms that the oscillation dominant frequencies are in the range of 0.1 to 3.0 Hz.
- The same PHP geometry and working conditions have been simulated for methanol, FC-72, and R123, and the model shows satisfactory qualitative and quantitative results.
- The present numerical model can be adapted to perform simulations also on multiturn CLPHP, which are proved to be an attractive solution for many industrial thermal management issues.

NOMENCLATURE

A	area, m^2
Bo	boiling number
c_p	specific heat, J/kg-K
d	diameter, m
f	friction factor
g	gravity acceleration, m/ s^2
h	heat transfer coefficient, W/m^2-K
H	specific enthalpy, J/kg
k	thermal conductivity, W/m-K
L	length, m
m	mass, kg
$\dot{m}$	mass flow rate, kg/s
Nu	Nusselt number
p	tube internal perimeter, m
P	pressure, Pa
ΔP	linear pressure drop, Pa/m
Pr	Prandtl number
q	heat flux, W/ m^2
$\dot{Q}$	heat input, W
R	ideal gas constant
Re	Reynolds number
R_{eq}	equivalent thermal resistance, K/W
r	radius, m
t	time, s
T	temperature, °C
$\bar{T}$	mean steady-state temperature, °C
V	volume, m^3
u	fluid velocity, m/s
x	vapor mass quality, kg_v/kg_t
z	axial direction coordinate, m

Greek Symbols

δ	thickness, m
ε	surface roughness, m
μ	dynamic viscosity, Pa.s
ρ	density, kg/m^3
σ	surface tension, N/m
θ	inclination angle, deg
τ	shear stress, N/m^2

Subscripts

b	back liquid slug meniscus
c	capillary
co	condenser/condensing
cr	flow cross section
$crit$	critical
ev	Evaporator
ex	external
f	front liquid slug meniscus
g	gravity
$film$	liquid film
i	liquid slug index
j	vapor plug index
l	liquid phase
lv	liquid–vapor
min	minimum
max	maximum
sat	saturated condition
v	vapor phase
vp	vapor plug
w	tube wall
$w\text{-}f$	wall to fluid
0	initial condition
∞	cooling medium

REFERENCES

[1] Vasiliev, L., Heat Pipes in Modern Heat Exchangers, *Applied Thermal Engineering*, vol. 25, pp. 1–19, 2005.

[2] Akachi, H., Structure of a Heat Pipe, US patent, No. 4,921,041, 1990.

[3] Akachi, H., Structure of a Micro Heat Pipe, US patent, No. 5,490,558, 1993.

[4] Akachi, H., Polášek, F., and Štulc, P., Pulsating Heat Pipes, *Proc. 5th International Heat Pipe Symposium*, pp. 208–217, Melbourne, Australia, 1996.

[5] Yang, H., Khandekar, S., and Groll, M., Performance Characteristics of Pulsating Heat Pipes as Integral Thermal Spreaders, *International Journal of Thermal Sciences*, vol. 48, pp. 815–824, 2009.

[6] Miyazaki, Y., Cooling of Notebook PCs by Flexible Oscillating Heat Pipes, *Proc. ASME INTERPACK*, San Francisco, CA, July 17–22, 2005.

[7] Rittidech, S., and Wannapakne S., Experimental Study of the Performance of a Solar Collector by Closed-End Oscillating Heat Pipe (CEOHP), *Applied Thermal Engineering International Journal*, vol. 27, pp. 1978–1985, 2007.

[8] Khandekar, S., Pulsating Heat Pipe Based Heat Exchangers, *Proc. 21st International Symposium on Transport Phenomena*, Kaohsiung City, Taiwan, 2–5 November, 2010.

[9] Zuo, Z. J., North, M. T., and Ray L., *Combined Pulsating and Capillary Heat Pipe Mechanism for Cooling of High Heat Flux Electronic*, Internal Report, Thermacore, Inc., Lancaster, PA, USA, 2001.

[10] Shafi, M. B., Faghri, A., and Zhang, Y., Thermal Modeling of Unlooped and Looped Pulsating Heat Pipes, *ASME Journal of Heat Transfer*, vol. 123, pp. 1159–1162, 2001.

[11] Zhang, Y., and Faghri, A., Oscillatory Flow in Pulsating Heat Pipes With Arbitrary Numbers of turns, *Journal of Thermophysics and Heat Transfer*, vol. 17, no. 3, pp. 340–347, 2003.

[12] Sakulchangsatjatai P., Chareonsawan, P., Waowaew, T., Terdtoon, P., and Murakami, M., Mathematical Modelling of Closed-End Pulsating Heat Pipes Operating With a Bottom Heat Mode, *Heat Transfer Engineering*, vol. 29, no. 3, pp. 239–254, 2008.

[13] Khandekar S., and Groll, M., Roadmap to Realistic Modeling of Closed Loop Pulsating Heat Pipes, *Proc. 9th International Heat Pipe Symposium*, Kuala Lumpur, Malaysia, November 2008.

[14] Holley, B., and Faghri, A., Analysis of Pulsating Heat Pipe with Capillary Wick and Varying Channel Diameter, *International Journal of Heat and Mass Transfer*, vol. 48, pp. 2635–2651, 2005.

[15] Khandekar, S., and Groll, M., An Insight Into Thermo-Hydrodynamic Coupling in Closed Loop Pulsating Heat Pipes, *International Journal of Thermal Sciences*, vol. 43, pp. 13–20, 2004.

[16] Shah, R. K., Thermal Entry Length Solutions for the Circular Tube and Parallel Plates, *Proc. 3rd National Heat and Mass Transfer Conference*, IIT Bombay, vol. I, Paper HMT-11–75, 1975.

[17] Incropera, F. P., and DeWitt, D. P., *Fundamentals of Heat and Mass Transfer,* 6th ed., Wiley, USA, 2007.

[18] Han Y., and Shikazono N., Measurement of the Liquid Film Thickness in Micro Tube Slug Flow, *International Journal of Heat and Fluid Flow*, vol. 30, pp. 842–853, 2009.

[19] Gungor K. E., and Winterton, R. K. S., Simplified General Correlation for Saturated Flow Boiling and Comparisons of Correlations With Data, *Chemical Engineering Research and Design*, vol. 65, pp. 148–166, 1987.

[20] Shah, M. M., A General Correlation for Heat Transfer During Film Condensation Inside of Pipes, *International Journal of Heat and Mass Transfer*, vol. 22, pp. 547–556, 1079.

[21] Lemmon, E. W., Huber, M. L., and McLinden, M. O., NIST Standard Reference Database 23: Reference Fluid Thermodynamic and Transport Properties-REFPROP, Version 8.0, National Institute of Standards and Technology, Standard Reference Data Program, Gaithersburg, 2007.

[22] Khandekar, S., Gautam, A. P., and Sharma, P. K., Multiple Quasi-Steady States in a Closed Loop Pulsating Heat Pipe, *International Journal of Thermal Sciences*, vol. 48, pp. 536–546, 2009.

[23] Yang, H., Khandekar, S., and Groll, M., Operational Limit of Closed Loop Pulsating Heat Pipe, *Applied Thermal Engineering*, vol. 28, pp. 49–59, 2008.

Mauro Mameli has been a Ph.D. student in energy and environment technologies at Bergamo University since 2009. He received his master's degree in mechanical engineering at Bergamo University and he is currently working on the numerical and experimental investigation of closed loop pulsating heat pipes.

Marco Marengo is an associate professor of industrial engineering, scholar of spray, injection, and liquid interfaces from 1993, directorate member of the European Institute for Liquid Atomization and Spray System (ILASS), European editor for the ILASS newsletter, local coordinator of national and European research projects in spray and micro heat exchangers topics, founder of the microfluidics laboratory at the Bergamo University, and author of 70 scientific papers.

Stefano Zinna is an expert in simulations of thermal control two-phase systems by using lumped parameter and distributed codes. He received his master's degree in mechanical engineering at Brescia University and his Ph.D. degree in energy and environment technologies at Bergamo University. Since 2004 he has been involved in many European and national projects, among them the AMS (alpha magnetic spectrometer) experiment. Since 2008 he has been the technical director for Uniheat S.r.l.